

# Enhanced Multi-Target Tracking in Dynamic Environments: Distributed Control Methods Within the Random Finite Set Framework

Aidan Blair<sup>a</sup>, Amirali K. Gostar<sup>a</sup>, Alireza Bab-Hadiashar<sup>a</sup>, Xiaodong Li<sup>a</sup>, Reza Hoseinnezhad<sup>a</sup>

<sup>a</sup>RMIT University, Melbourne, VIC, Australia

## Abstract

Tracking multiple targets in dynamic environments using distributed sensor networks is a challenging problem that has received significant attention in recent years. In such scenarios, the network of sensors must coordinate their actions to estimate the locations and trajectories of multiple targets accurately. Multi-sensor control methods can improve the performance of these networks by enabling efficient utilization of resources and enhancing the accuracy of the estimated target states. This paper proposes two novel multi-sensor control methods that utilize the Random Finite Set (RFS) framework to address this problem. Our methods improve computational tractability and enable fully distributed control, making them suitable for real-time applications.

**Keywords:** distributed sensor network, sensor control, genetic algorithm, random finite sets, flooding

## Symbols & Notation

Symbol	Definition or meaning
$s$	index or label of a controllable sensor node in the distributed sensor network
$N(s)$	The collection of all sensor nodes in the network that can communicate with node $s$
$N_s$	total number of sensor nodes in the overall distributed sensor network
$k$	time: index of multi-object filtering iteration at each sensor node (different at each sensor node, for asynchronous communication)
$\pi_{k,s}$	the multi-object random finite set density at time $k$
$\pi_{k k-1,s}$	the predicted multi-object density at filtering time $k$
$r_{k,s}^{(\ell)}$	probability of existence of the object labeled $\ell$ according to the LMB posterior formed in sensor node $s$ at filtering time $k$
$p_{k,s}^{(\ell)}(\cdot)$	state density of the object labeled $\ell$ (conditional on its existence), according to the LMB posterior formed in sensor node $s$ at filtering time $k$
$\hat{X}_{k k-1,s}$	the set of objects estimated to exist from the predicted multi-object density at time $k$ in sensor node $s$
$Z_{k,s}$	set of measurements yielded from sensor $s$ at time $k$ , after sensor control command $u_{k,s}^*$ is executed
$p_{s,k}^d(x)$	probability of an object with state $x$ to be detected by the sensor in node $s$ at time $k$
$\rho_{\max}$	maximum detectable range (sensor-object distance)
$\theta_{\max}$	half of the total angular width of sensor's field-of-view
$\mathbb{U}$	the finite set of all permissible single-sensor commands, $u$
$u_{k,s}^*$	the optimal single-sensor command concluded at sensor node $s$ for its own execution at time $k$ before measurement acquisition
$u_s = (u_1, \dots, u_{N(s)})$	a multi-sensor command in $\mathbb{U}^{N(s)}$ , hypothesized at sensor node $s$

Preprint submitted to Elsevier

January 26, 2024

Symbol	Definition or meaning
$\tilde{Z}_{k,s}(u)$	the predicted ideal measurement set (PIMS) computed at sensor node $s$ after the command $u$ is hypothetically applied
$\tilde{\pi}_{k,s}(\cdot; u)$	the pseudo-posterior returned by running the update step in node $s$ at time $k$ , using the PIMS $\tilde{Z}_{k,s}(u)$ as measurement set
$\pi_{\text{fused},k,s}$	the outcome of fusion of all the posteriors formed in sensor $s$ and its neighbors, at time $k$
$v(\tilde{\pi}_{\text{fused},k,s}, \pi_{k k-1,s})$	the multi-sensor control reward value as an information divergence function from the predicted posterior to the fused pseudo-posterior in sensor node $s$ at time $k$
$v(\tilde{u}_{k,s})$	the multi-sensor control reward value as a function of the hypothesized multi-sensor command in sensor node $s$ at time $k$
$ X $	cardinality (number of elements) of a set $X$
$t$	index or counter to the information flooding iterations locally occurring in each sensor node during a single filtering iteration

## 1. Introduction

This article addresses the challenge of distributed multi-sensor control for multi-target tracking. Generally, the challenge encompasses a distributed network of sensors where each node of the network communicates with its neighbors. Every sensor captures measurements pertinent to the targets within its field of view (FoV) and executes a stochastic multi-target filter on board which produces a multi-object posterior. The posterior probabilities are then transmitted and received through the network and fused locally at each sensor node. In this context, the issue of multi-sensor control emerges when the state of the sensors can be altered using control commands. In most instances, the sensor states are defined by their location and orientation, and a change in their state signifies *movement*.

An instance illustrating the utilization of multiple sensors mounted on Unmanned Air Vehicles (UAVs) for inspecting the sea surface to detect and track sea vessels is depicted in Figure 1. In this illustration, each UAV is required to autonomously determine its subsequent actions (in terms of transitioning to a new location and orientation), relying on hypothesized future movements of other UAVs within the network. The decision must be made in a manner that optimizes the acquisition of *most informative* measurements by the interconnected UAV network, aiming to obtain a situational awareness that is as comprehensive as possible.

Multi-sensor control is a complex and critical area of research that has gained significant attention in various fields, including but not limited to autonomous vehicle networks [1], surveillance and intelligence applications [2], and defense applications of multi-target tracking [3]. In all such applications, a network of sensors are used to acquire and fuse information for situational awareness. Depending on how information is communicated in the network, it may be characterized as a centralized, decentralized, or distributed sensor network [4, 5].

Centralized networks are composed of a central processing node that communicates with every other node in the network. The central node gathers data from all the other nodes, processes it, and distributes the results back to the other nodes. In decentralized networks, nodes form local clusters, with each cluster containing a central node that communicates with the other nodes in the cluster. Additionally, these central nodes can communicate with other central nodes in the network, facilitating information transfer throughout the network. Distributed networks lack central processing nodes. Instead, nodes can only communicate with their nearest neighbors, usually within a limited communication range.

Distributed networks are commonly divided into two categories with regard to inter-node communication: consensus and flooding. In consensus-based communication, the nodes in the network collaborate to reach an agreement or consensus on a certain value or state. This involves

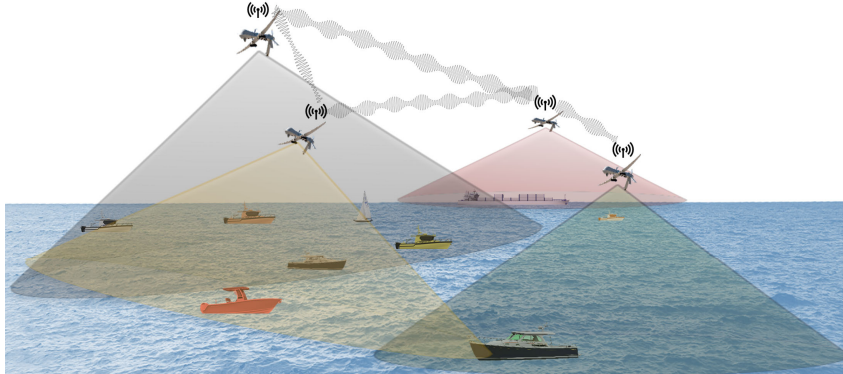


Figure 1: Multiple unmanned air vehicles (UAVs) must cooperatively inspect part of the ocean for monitoring of marine vehicles on the sea surface.

iterative exchanges of information among nodes until they converge to a common decision. Consensus algorithms aim to achieve agreement while minimizing information exchange and communication overhead [6, 7]. Flooding involves broadcasting information from a source node to all other nodes in the network. Each node that receives the broadcasted information will then forward it to all of its neighbors. This process continues until all nodes in the network have received the information [8, 9].

Distributed networks offer a pragmatic solution for the implementation of large-scale sensor networks, as the computational cost of centralized networks tends to grow exponentially with each added sensor. Distributed networks, on the other hand, can readily adapt to the integration of more sensors, enabling the system to scale without incurring excessive computational burden. In practical applications with large sensor networks, distributed communication and computing is the preferred option. Hence, we focus on distributed multi-sensor control.

As mentioned earlier, our proposed solution is for applications where sensor information needs to be fused for multi-target tracking. Random Finite Sets (RFS) is a powerful Bayesian framework for multi-target tracking, wherein the sets of target states and observations are represented as random finite sets. A number of filters have been developed in this framework, including the well-known probability hypothesis density (PHD) [10] and multi-Bernoulli (MeMBer) [11] filters. The latest development in RFS filters, called *labeled RFS filters*, appends the label of each target into its single-target state and propagates target labels with their states to directly create *target trajectories* [12, 13, 14]. RFS filters have found applications in various fields, including cell lineage tracking [15], intelligent transport systems (ITS)[16], and information fusion[17, 18], especially in multi-target tracking applications.

Various sensor control methods have been proposed for Random Finite Sets (RFS) filters using different objective functions [19, 20, 21, 22]. However, these methods have mainly been explored in single-sensor control scenarios. Recent works have introduced multi-sensor control for labeled RFS filters. For instance, Jiang et al. [23] proposed a Cauchy-Schwarz divergence-based objective function combined with Generalized Labeled Multi-Bernoulli (GLMB) filters. Another example is the multi-sensor control solution in which a task-driven cost (which is a mixture of the expected localization and cardinality errors) was chosen to be minimized [24]. In this work, a Labeled Multi-Bernoulli (LMB) filter was assumed to be running on board each sensor node. Panicker et al. [25] developed a multi-sensor control solution that focuses on targets

of interest, again with LMB filters running on each node. An information-theoretic objective function for RFS-based multi-sensor control was also proposed [26].

This paper is a significant extension of a previous work [27] that introduces the problem of distributed multi-sensor control with LMB filters running at each sensor node of the network. The original solution was an algorithm that employs distributed coordinate descent on sensor neighborhoods. In this paper, we introduce two innovative distributed multi-sensor control algorithms that are specifically devised to work with LMB filters running at each sensor node.

- The first solution, called GA-SC, is based on a genetic algorithm optimization approach for determining multi-sensor control commands.
- The second solution, called DF-SC, is a distributed flooding-based multi-sensor control algorithm.

Our proposed methods demonstrate exceptional performance in comparison to prevailing techniques while concurrently achieving a substantial reduction in computational complexity. The rest of this paper is outlined as follows:

Section 2 offers an overview of current multi-sensor control methods with a focus on RFS filter-based approaches. In Section 3, we provide background information on the RFS framework and state the problem of multi-sensor control within the general distributed multi-target tracking application. Section 4 presents our proposed solutions, followed by Section 5 where the findings of the numerical experiments we have conducted to benchmark the performance of our methods against state-of-art, are presented. Finally, Section 6 concludes the paper.

## 2. Related Work

In the RFS framework, various solutions have been developed for multi-target tracking-related problems. Some examples include track-before-detect visual tracking applications [28], sensor management in target tracking applications [25, 29], and information fusion [30]. Several information fusion approaches have been explored for applications with LMB filters in place as tracking solution, ranging from Cooperative Cauchy-Schwarz divergence-based fusion [31] to Consensus-based fusion [32] and Complementary fusion [33].

The communication between sensors in a distributed sensor network has been the subject of significant research, but distributed multi-sensor control has not received as much attention. Akselrod and Kirubarajan [34] proposed a distributed control algorithm for multi-target tracking by a swarm of UAVs. In this algorithm, measurements and associated tracks from each UAV are broadcast throughout the network and fused with the local measurements at each UAV using Markov Decision Processes to communicate information optimally over the network. However, each UAV chooses an action to take without considering the actions of other UAVs, which could lead to multiple nearby UAVs converging on the same target. This approach is counterproductive in a large distributed network. To address this issue, Fu and Yang [35] proposed a control framework aimed at maximizing tracking accuracy while guaranteeing tracking coverage. Each sensor can be allocated to track a particular target or group of targets, and sensor positions and allocations are shared distributively throughout the network to jointly optimize for tracking accuracy while ensuring that at least one sensor is allocated to every target.

Yuan, Zhan, and Li [36] use a distinct approach by achieving flocking in quadcopter UAVs in a decentralized manner. Each UAV shares its local information with neighboring nodes, which is then used by a decentralized model predictive control (DMPC) flocking algorithm to form a quasi

$\alpha$ -lattice. In this application, sensors have access to information only from their neighboring sensors, which limits their ability to form a fully accurate lattice and results in a quasi-lattice formation.

Machine learning-based multi-sensor control techniques have been increasingly explored for multi-target tracking applications. One such application involves controlling unmanned aerial vehicles (UAVs) using deep reinforcement learning, as described in [37]. In this work, multi-agent reinforcement learning is utilized to compute actions for multiple sensors, incorporating a decentralized approach. However, despite its decentralized aspects, this approach still relies on a centralized reinforcement learning network. Specifically, while local observations, updates, and initial action selection are performed by individual sensors, the final sensor actions are determined by broadcasting these data to a central reinforcement learning network, which computes the actions.

Coordinate Descent is a family of optimization techniques where each dimension/parameter is optimized sequentially while the others are kept fixed, approximately optimizing along coordinate directions. An overview of various coordinate descent algorithms is provided by Wright [38]. Wang et al. [24] proposed a method for multi-sensor control of RFS filters using coordinate descent. Richtárik & Takáč [39] proposed a form of distributed coordinate descent in datasets with a high number of dimensions, where the dimensions are partitioned among a network of computers so that each computer solves a subset of the overall problem. After local convergence, the locally updated vectors are distributed among the network, and the process is repeated until convergence. Yang & Gajwa [40] have implemented a robust form of distributed coordinate descent for distributed machine learning applications. Their approach is tolerant to Byzantine faults, which are a significant challenge in distributed computing, allowing for the practical implementation of distributed machine learning algorithms. Recently, a coordinate descent-based method for multi-sensor control in multi-target tracking applications has been developed [27].

Genetic Algorithms are stochastic population-based optimization methods, based on the principles of natural selection [41]. They do not require gradient information and are generic and more robust (i.e. less likely to get stuck in local optima), and can be applied to a wide range of optimization problems. Numerous control algorithms across many fields have used genetic algorithms for optimization, including UAV control [42], manufacturing [43] and wireless sensor networks [44].

### 3. Problem Statement and Background

#### 3.1. Overall architecture

Figure 2 provides a general overview of the entire sequence of operations executed by each sensor node,  $s$ , in a distributed sensor network. For every filtering time instance  $k$ , the node carries out the prediction step of its multi-object filter, both on its own multi-object prior,  $\pi_{k-1,s}$ , and on the latest multi-object posterior densities,  $\pi_{k-1,s'}$ , obtained at the previous filtering time  $k-1$  from all adjacent sensor nodes  $s' \in N(s)$ , where  $N(s)$  denotes the collection of all neighboring nodes that transceive inform with node  $s$ .

The primary focus of this work is the design of a solution for the *multi-sensor control* block, highlighted in red. This block takes as input all the predicted multi-object densities,  $\pi_{k|k-1,s'}$ ,  $s' \in N(s) \cup \{s\}$ , and then determines the *optimal* control command (such as movement or rotation),  $u_{k,s}^*$ , for sensor node  $s$ . Following this, the system executes the control command on the sensor (e.g.,

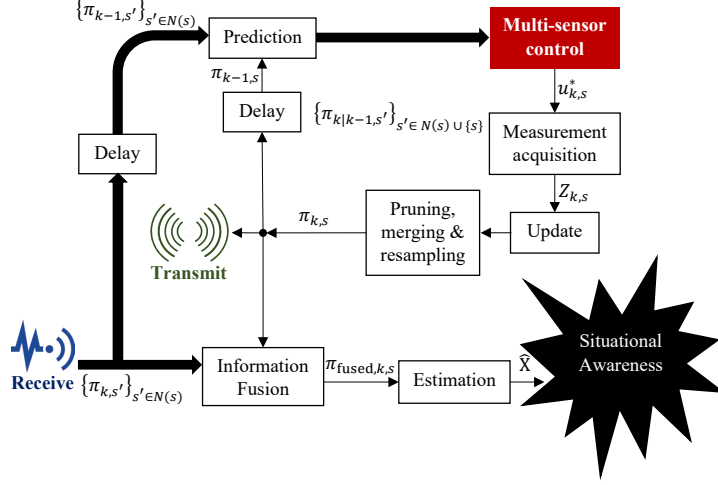


Figure 2: Overall operations running onboard each sensor node  $s$ , for tracking and control.

moving or rotating it as required) and subsequently performs detection, yielding a measurement set  $Z_{k,s}$ . This set is utilized to update the predicted density, resulting in the local posterior  $\pi_{k,s}$ .

The obtained local posterior is then transmitted to all neighboring sensors and serves as the local multi-object prior for the next time step. To achieve situational awareness regarding the number and states of objects of interest, each node fuses its local posterior with all received posteriors. It then estimates the multi-object state from the fused posterior.

### 3.2. System components and model assumptions

The prominent component of the overall architecture shown in Figure 2 is the *multi-object filter* running at each node. Before the filter of choice is presented, some notation and assumptions need to be clarified.

For a multi-object system presented in discrete time  $k$ , the multi-object state  $X_k$  can be described by a labeled random finite set (RFS) composed of several single-object states,

$$X_k = \{(x_{1,k}, \ell_1), \dots, (x_{N_s,k}, \ell_{N_s})\} \in \mathcal{F}(\mathbb{X} \times \mathbb{L}) \quad (1)$$

where each state  $x$  has been augmented with a label  $\ell$ . At each discrete filtering time step  $k$ , each sensor node  $s$  of the network returns a set of measurements that may include object detections and false alarms (clutter).

The probability of detection of an object with state  $x$  is denoted by  $p_{s,k}^d(x)$ , implying that it may differ from one sensor node to another, may vary with time and may be dependent on the object's state. The dependence on object's state is particularly of interest and significance. The *limits* of the sensor's field of view is mathematically formulated by incorporating such a dependency. An example is shown in Figure 3. In a 2D tracking application, the sensor is looking downward at a tilt angle  $\theta_s$ . Its field of view is limited in range (can only detect objects at distances between  $\rho_{\min}$  and  $\rho_{\max}$ ) and angle (up to  $\theta_{\max}$  radians away from sensor's tilted axis). Having the sensor

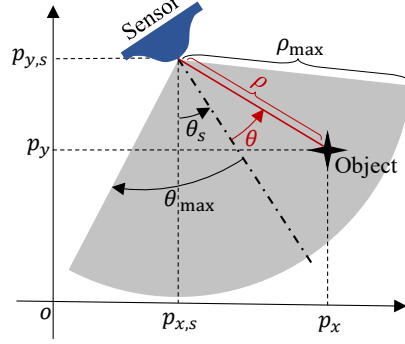


Figure 3: Schematic diagram of a sensor with limited FoV, and the notation used for formulation of the probability of detection.

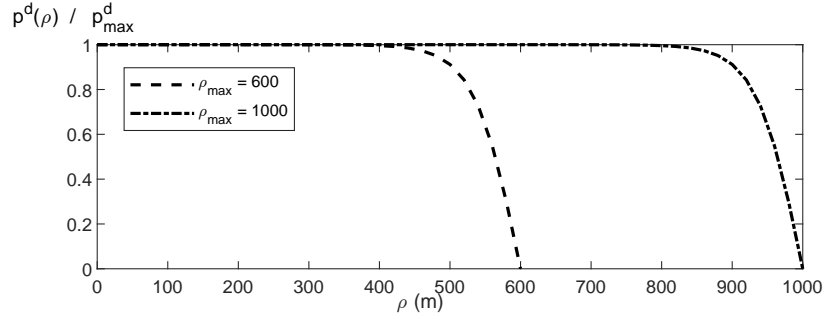


Figure 4: Probability detection variations against range for two cases in both of which  $\rho_{\min} = 0$  and  $\lambda = 65$  m, but maximum range is 600 m in one scenario and 1000 m in another

located at  $(p_{x,s}, p_{y,s})$ , the probability of detection of an object located at  $(p_x, p_y)$  can be given by:

$$p_s^d(\rho, \theta) = \begin{cases} p_{\max}^d \frac{\tanh\left(\frac{[\rho_{\max} - \rho]}{\lambda}\right)}{\tanh\left(\frac{[\rho_{\max} - \rho_{\min}]}{\lambda}\right)} & \text{if } |\theta| \leq \theta_{\max} \text{ and } \rho \leq \rho_{\max} \\ 0 & \text{else} \end{cases} \quad (2)$$

where

$$\rho = \sqrt{(p_x - p_{x,s})^2 + (p_y - p_{y,s})^2}, \quad \theta = \text{atan2}(p_x - p_{x,s}, p_y - p_{y,s}) + \frac{\pi}{2} - \theta_s$$

where atan2 means the four-quadrant inverse tangent function.

Figure 4 shows how the  $p_s^d$  values given by the above model vary from the maximum value to zero as the sensor-object distance increases up to the maximum range.

Conditional on detection, the sensor  $s$  is assumed to provide a measurement  $z$  that is distributed according to a density given by the likelihood function  $g_s(\cdot|x, x_s)$  where  $x$  is the detected object's state, and  $x_s$  denotes the sensor's state (e.g. its location  $(p_{x,s}, p_{y,s})$  and orientation  $\theta_s$  as shown in Figure 3). Each sensor can be controlled via a sensor control command  $u_s^* \in \mathbb{U}$  where  $\mathbb{U}$  is a finite set of sensor control commands. Obviously, the sensor's state will depend on what control

action is chosen and executed. Hence, the measurement likelihood values will be dependent on sensor control actions too. A multi-sensor control command can be constructed by appending multiple single-sensor control commands,  $u = (u_1, \dots, u_{N_s}) \in \mathbb{U}^{N_s}$ .

The overarching aim of controlling a set of sensors for multi-object tracking is to substantially improve the accuracy of target state estimation. This encompasses refining both the detection of the total number of targets (cardinality) and the detailed assessment of each target's specific attributes, such as position, velocity, and orientation.

### 3.3. The multi-object filter

As was emphasized previously, a multi-object filter runs onboard each sensor node. The Bayesian multi-object filter propagates the multi-object density through its prediction and update steps, and after the posterior is fused with other similar posteriors received from neighboring nodes, it extracts the multi-object estimate, which is our realization of situational awareness. The distributed multi-sensor control solution proposed in this paper can be applied with almost any choice of RFS-based multi-object filter. However, due to its proven performance and intuitive structure, we present and formulate our solution for applications where the labeled multi-Bernoulli (LMB) filter [14] is locally running in each node.

The LMB distribution is completely described by its components  $\pi = \{(r^{(\ell)}, p^{(\ell)}(\cdot))\}_{\ell \in \mathbb{L}}$  where  $r^{(\ell)}$  is the probability of the existence of an object with label  $\ell \in \mathbb{L}$ , and  $p^{(\ell)}(x)$  is the probability density of the object state conditional on its existence. Mathematically, for any multi-object state  $X = \{(x_1, \ell_1), \dots, (x_n, \ell_n)\}$ , the multi-object density is given by

$$\pi(X) = \begin{cases} \omega(\{\ell_1, \dots, \ell_n\}) \prod_{i=1}^n p^{(\ell_i)}(x_i) & \text{if } \forall i, j \in [1, n], i \neq j \Rightarrow \ell_i \neq \ell_j \\ 0. & \text{else} \end{cases} \quad (3)$$

where

$$\omega(L) = \prod_{\ell \in L} r^{(\ell)} \prod_{\ell \in (\mathbb{L} - L)} (1 - r^{(\ell)}) \quad (4)$$

is the probability of joint existence of all objects with labels  $\ell \in L$  and non-existence of all other labels. For computing single-object densities, a particle implementation is used in this paper, where the density of each LMB component with label  $\ell$  is approximated by  $J^{(\ell)}$  weights and particles,  $p^{(\ell)}(x) \approx \sum_{j=1}^{J^{(\ell)}} w_j^{(\ell)} \delta(x - x_j^{(\ell)})$  where  $\delta(\cdot)$  is the Dirac delta function. Note that the proposed multi-sensor control solution could be used with Gaussian-mixture implementation in a similar manner.

### 3.4. Information fusion

As shown in Figure 2, *information fusion* is a critical task that needs to be completed in each sensor node. With limited field of view, we need a *complementary* fusion method that puts together all the information gathered by various sources. We have already developed such a solution tailored for fusion of several LMB posteriors [30] but in a centralized sensor network. In this paper, we propose a slightly varied version that can be directly applied in a distributed sensor network.

Referring to Figure 2, assume that the multiple LMB densities that need to be fused are parametrized as follows:

$$\pi_{k,s} = \left\{ \left( r_{k,s}^{(\ell)}, p_{k,s}^{(\ell)}(\cdot) \right) \right\}_{\ell \in \mathbb{L}_{k,s}}, \quad \text{and for } s' \in N(s) : \pi_{k,s'} = \left\{ \left( r_{k,s'}^{(\ell)}, p_{k,s'}^{(\ell)}(\cdot) \right) \right\}_{\ell \in \mathbb{L}_{k,s'}}.$$



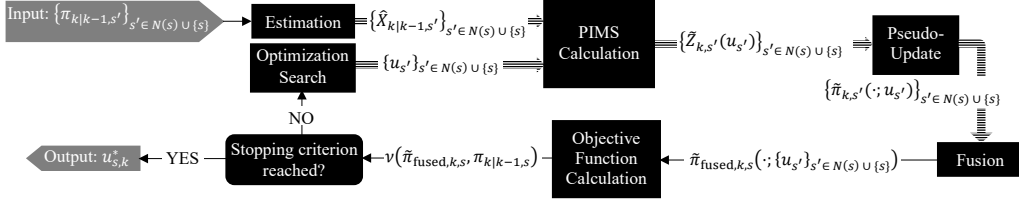


Figure 5: The proposed architecture of the contents of multi-sensor control block executing at sensor node  $s$ , in the overall schematics shown in Figure 2.

Two important notes should be made here. Firstly, the space of object labels (detected by each sensor up to time  $k$ ) may be different in each node due to limited fields of view.

Secondly, if the single-object densities are approximated by particles, for each label, the fused single-object density will be approximated by all the particles from different sensors for that label. The particle weights will need to be re-scaled according to the probability of existence reported by each sensor for that label.

For any node  $s' \in N(s) \cup \{s\}$ , let us assume that at time  $k$ , single-object density associated with label  $\ell$  is approximated by  $J_{k,s'}^{(\ell)}$  pair of particles and weights, where the  $j$ -th pair is denoted by  $(x_{j,k,s'}^{(\ell)}, w_{j,k,s'}^{(\ell)})$ . The fused density at node  $s$ ,  $p_{\text{fused},k,s}^{(\ell)}(\cdot)$  will then be represented by  $J_{\text{fused},k,s}^{(\ell)} = \sum_{s' \in N(s) \cup \{s\}} J_{k,s'}^{(\ell)}$  pairs of particles and weights denoted by the union of individual sets of particles and weights, as follows:

$$p_{\text{fused},k,s}^{(\ell)}(x) \approx \sum_{s' \in N(s) \cup \{s\}} \sum_{j=1}^{J_{k,s'}^{(\ell)}} [\alpha_{k,s'}^{(\ell)} w_{j,k,s'}^{(\ell)}] \delta(x - x_{j,k,s'}^{(\ell)}) \quad (5)$$

where the scaling factors  $\alpha_{k,s'}^{(\ell)}$  are proportional to probabilities of existence, i.e.

$$\alpha_{k,s'}^{(\ell)} = r_{k,s'}^{(\ell)} / \sum_{s \in N(s) \cup \{s\}} r_{k,s}^{(\ell)}.$$

To fuse the probabilities of existence for label  $\ell$  at each node, the individual probabilities of existence are combined according to the complementary fusion rule [30]:

$$r_{\text{fused},k,s}^{(\ell)} = q_{k,s}^{(\ell)} / \left[ 1 + \sum_{s' \in N(s) \cup \{s\}} q_{k,s'}^{(\ell)} \right] \quad (6)$$

where  $q_{k,s'}^{(\ell)} = r_{k,s'}^{(\ell)} / [1 - r_{k,s'}^{(\ell)}]$ . Note that pruning and resampling the particles will ensure numerical tractability.

#### 4. Distributed Multi-Sensor Control: The Proposed Solution

In this section, we present our proposed multi-sensor control solution for distributed multi-target tracking, in a step-by-step fashion. Figure 5 shows a block diagram of our proposed solution, in a form that could be the contents of the “Multi-sensor Control” block in Figure 2.

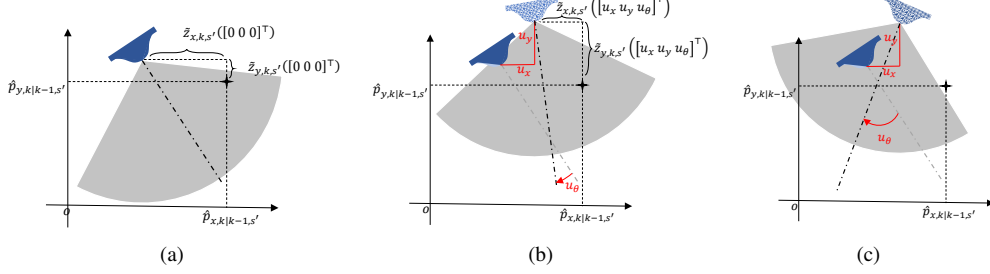


Figure 6: PIMS measurement returned for an object with hypothesized (a) zero control command, (b) a non-zero translation and rotation control command, and (c) another control command with the translation being same as in (b) but larger rotation that leads to the object being missed.

#### 4.1. Estimation

The first step is to *estimate* the number of objects and their states from the predicted densities at the local node  $s$  and received from the neighboring nodes  $s' \in N(s)$ . We choose the Expected A Posteriori (EAP) estimates. In the case of LMB densities, assuming that  $\pi_{k|k-1,s'}$  is parametrized as  $\left\{ \left( r_{k|k-1,s'}^{(\ell)}, \left\{ \left( w_{j,k|k-1,s'}, x_{j,k|k-1,s'} \right)_{j=1}^{J_{k-1,s'}^{(\ell)}} \right\} \right)_{\ell \in \mathbb{L}_{k-1,s'}}$  the EAP estimate for number of objects (cardinality) is given by the sum of all probabilities of existence,

$$|\hat{X}|_{k|k-1,s'} = \sum_{\ell \in \mathbb{L}_{k-1,s'}} r_{k|k-1,s'}^{(\ell)}. \quad (7)$$

The objects predicted to exist are then chosen as those with the highest probabilities of existence, up to  $|\hat{X}|_{k|k-1,s'}$  objects. For each chosen label  $\ell$ , the EAP estimate for state is given by:

$$\hat{x}_{k|k-1,s'}^{(\ell)} = \sum_{j=1}^{J_{k-1,s'}^{(\ell)}} w_{j,k|k-1,s'} x_{j,k|k-1,s'}. \quad (8)$$

#### 4.2. Calculation of the predicted ideal measurement set (PIMS)

The next step is to compute hypothesized measurements sets that could ideally be returned by each sensor node. Such sets are *ideal* in the sense that they include no measurement noise, false alarm or miss-detection, and correspond to all the objects estimated to be existing. An example is shown in Figure 6. Consider an object that is predicted by sensor node  $s'$ , to exist at an estimated location of  $(\hat{p}_{x,k|k-1,s'}, \hat{p}_{y,k|k-1,s'})$ . As shown in Figure 6(a), without any sensor action (zero control command), ideally the object would be detected, returning a measurement that is comprised of the horizontal and vertical distance from the object to the sensor, denoted by  $\tilde{z} = (\tilde{z}_{x,k,s'}, \tilde{z}_{y,k,s'})$ . If a hypothesized control command in the form of a 2D translation and rotation is applied to the sensor, the measurements will change – see Figure 6(b). Due to the sensor's limited field-of-view, it is also possible that a predicted object is entirely missed by the sensor – see Figure 6(c).

### 4.3. Pseudo-update and fusion

Once the PIMS are generated for each sensor node (self and neighboring nodes), a pseudo-update step is run. It is called “pseudo” due to the hypothetical nature of the measurements generated with zero noise for hypothetical control actions. The results are the multi-object posteriors that would be generated locally in each sensor node should the measurements locally acquired by those nodes were the PIMS generated in node  $s$  for them.

The pseudo-posteriors are then fused using the same fusion scheme that would be used in the update step after actual measurement acquisition by the sensor. In our experiments, with LMB filters running in each sensor node, fusion rules (6) and (5) are used, as also used in the update step.

### 4.4. Objective Function

The pseudo-posterior densities and their fused density are clearly dependent on the pseudo-measurements which are themselves dependent on the selected control commands,  $\mathbf{u}_s = \{\mathbf{u}_{s'}\}_{s' \in N(s) \cup \{s\}}$ . The fused pseudo-posterior is input to an objective function, which is at the core of optimizing the sensing performance through sensor control. It returns a scalar value, and should be formulated in such a way that its optimal value (its minimum if formulated as a cost function, or maximum if formulated as a reward function) is associated with the *best statistically expected* sensing performance.

Generally, two types of objective functions have appeared in the sensor control literature: the *task-driven* and the *information-driven*. The former type are usually defined to directly optimize a particular aspect of tracking. For instance, in some applications, the highest priority is given to the *coverage* aspect. Having a network of sensors with limited fields of view, distributing the sensors for maximum coverage could be achieved by choosing the *cardinality estimate* returned by the fused pseudo-posterior. The resulting sensor control solution, originally designed for one sensor, is called “Posterior Expected Number of Targets” (PENT) [45]. Alternatively, estimation of tracking error could be the particular aspect of the tracking task being optimized by sensor control. In that case, the objective function would be formulated as a cost function dependent on the expected error of estimation or tracking after a sensor action is taken [46, 20, 47]. Minimizing such task functions leads to selecting the action that is statistically expected to return minimum error.

Information-driven objective functions are usually information-theoretic reward functions designed to maximize the expected *information gain* from the prior density to the posterior after a sensor action has been taken. Information gain is usually quantified using an information divergence from the prior to posterior. The most commonly used divergences in stochastic sensor control are Rényi Divergence [48, 22] and Cauchy-Shwarz Divergence [31, 23, 26].

In this work, we propose use an objective function based on the Kullback-Leibler Divergence (KLD). Referring to the notation used in Figure 5, consider two multi-object densities formed in a node  $s$  at time  $k$ ; one being the prior  $\pi_{k|k-1,s}(\cdot)$  and the other being the fused pseudo-posterior  $\tilde{\pi}_{\text{fused},k,s}(\cdot; \mathbf{u}_s)$  which depends on a chosen multi-sensor control action  $\mathbf{u}_s$ . The sensor control objective function is then the reward associated with choosing  $\mathbf{u}_s$ , quantified by computing the KLD from the prior to the fused pseudo-posterior:

$$\begin{aligned} \nu(\pi_{k|k-1,s}(\cdot), \tilde{\pi}_{\text{fused},k,s}(\cdot; \mathbf{u}_s)) &= D_{\text{KL}}(\tilde{\pi}_{\text{fused},k,s}(\cdot; \mathbf{u}_s) \parallel \pi_{k|k-1,s}(\cdot)) \\ &= - \int_{\mathbb{X}} \tilde{\pi}_{\text{fused},k,s}(X; \mathbf{u}_s) \log \left( \frac{\tilde{\pi}_{\text{fused},k,s}(X; \mathbf{u}_s)}{\pi_{k|k-1,s}(X)} \right) \delta X. \end{aligned} \quad (9)$$

In the case that both densities are LMB, denoting them by:

$$\tilde{\pi}_{\text{fused},k,s} = \left\{ \left( \tilde{r}_{\text{fused},k,s}^{(\ell)}, \tilde{p}_{\text{fused},k,s}^{(\ell)} \right) \right\}_{\ell \in \mathbb{L}_{k,s}}, \quad \pi_{k|k-1,s} = \left\{ \left( r_{k|k-1,s}^{(\ell)}, p_{k|k-1,s}^{(\ell)} \right) \right\}_{\ell \in \mathbb{L}_{k|k-1,s}}$$

the integral has a closed form given by [49]:

$$\begin{aligned} v \left( \pi_{k|k-1,s}(\cdot), \tilde{\pi}_{\text{fused},k,s}(\cdot; \mathbf{u}_s) \right) &= \sum_{\ell \in \mathbb{L}_{k|k-1,s}} \left[ \tilde{r}_{\text{fused},k,s}^{(\ell)} \log \left( \frac{\tilde{r}_{\text{fused},k,s}^{(\ell)}}{r_{k|k-1,s}^{(\ell)}} \right) + [1 - \tilde{r}_{\text{fused},k,s}^{(\ell)}] \times \right. \\ &\quad \left. \log \left( \frac{1 - \tilde{r}_{\text{fused},k,s}^{(\ell)}}{1 - r_{k|k-1,s}^{(\ell)}} \right) + \tilde{r}_{\text{fused},k,s}^{(\ell)} D_{\text{KL}}(\tilde{p}_{\text{fused},k,s}^{(\ell)} \| p_{k|k-1,s}^{(\ell)}) \right]. \quad (10) \end{aligned}$$

In distributed tracking involving sensors with limited field of view, usually *maximum coverage* is the major intended outcome of multi-sensor control. Consequently, the significance of information gain through single-object densities with sharper peaks (the last term in (10)) is negligible compared to the information gain through fused probabilities of existence that convey more confidence (are closer to 0 or 1). Therefore, the last term of the reward function (10) can be ignored to significantly speed up computation with no noticeable reduction in sensor control performance.

Additionally, we add a penalty when a target label is included in the prior but not in the pseudo-posterior, i.e. when the actions result in a target no longer being observed. This emphasizes actions that do not result in targets being dropped. The penalty term is formulated as the sum of  $\log(1 - r_{k|k-1,s}^{(\ell)})$  over all labels  $\ell \in [\mathbb{L}_{k|k-1,s} - \mathbb{L}_{\text{fused},k,s}]$ . Note that this penalty term negates the second term in equation (10),  $[1 - \tilde{r}_{\text{fused},k,s}^{(\ell)}] \log((1 - r_{k|k-1,s}^{(\ell)}) / (1 - \tilde{r}_{\text{fused},k,s}^{(\ell)}))$  when  $\tilde{r}_{\text{fused},k,s}^{(\ell)}$  equals zero.

Overall, our proposed objective function is given by:

$$\begin{aligned} v \left( \pi_{k|k-1,s}(\cdot), \tilde{\pi}_{\text{fused},k,s}(\cdot; \mathbf{u}_s) \right) &= \sum_{\ell \in \mathbb{L}_{k|k-1,s}} \left[ \tilde{r}_{\text{fused},k,s}^{(\ell)} \log \left( \frac{\tilde{r}_{\text{fused},k,s}^{(\ell)}}{r_{k|k-1,s}^{(\ell)}} \right) + [1 - \tilde{r}_{\text{fused},k,s}^{(\ell)}] \times \right. \\ &\quad \left. \log \left( \frac{1 - \tilde{r}_{\text{fused},k,s}^{(\ell)}}{1 - r_{k|k-1,s}^{(\ell)}} \right) \right] + \sum_{\ell \in [\mathbb{L}_{k|k-1,s} - \mathbb{L}_{\text{fused},k,s}]} \log(1 - r_{k|k-1,s}^{(\ell)}). \quad (11) \end{aligned}$$

#### 4.5. Optimization and stopping criterion

A different choice of the multi-sensor control command,  $\mathbf{u}_s = \{u_{s'} \in \mathbb{U}\}_{s' \in N(s) \cup \{s\}}$ , would generate a different set of fused pseudo-updated probabilities of existence, and therefore a different value for the reward function (11). The ultimate aim is to find the optimal multi-sensor control command at each sensor node that would return *maximum* reward. Denoting the optimal command by  $\mathbf{u}_s^* = \{u_{s'}^*\}_{s' \in N(s) \cup \{s\}}$ , the algorithm only outputs the one element  $u_s^*$  at each node  $s$  which is then executed to move the sensor before actual measurement acquisition.

The optimization search is an iterative procedure which stops when a particular criterion is met. In this work, we propose two different solutions for implementing the optimization search and choosing the stopping criterion. The first solution is based on genetic algorithms, and the

second one is based on using a distributed flooding procedure for convergence. The next two sections present the details of those approaches.

### **Distributed Genetic Algorithm-Based Multi-Sensor Control (GA-SC)**

A practical imperative when performing sensor control in real-time distributed multi-target tracking is narrowing the search space of possible actions to make the problem computationally tractable. Similar to our previous work [27], we propose that each sensor locally generates a multi-sensor control command for itself and its neighbors. However, rather than optimizing using coordinate descent, a genetic algorithm is used [41].

At each node  $s$ , the multi-sensor command is initialized as an all-one vector,

$$\mathbf{u}_s = \underbrace{[1, \dots, 1]}_{1+|N(s)|}. \quad (12)$$

Note that with the sensor command space  $\mathbb{U}$  assumed to be finite, possible single-sensor commands  $u \in \mathbb{U}$  are coded into an integer, starting with ‘1’ being the code for the sensor’s state to remain unchanged (stationary). So, the multi-sensor command is initialized to “all sensors remaining stationary”. This is then iteratively evolved into having other possible commands included. For instance, if there are  $|N(s)| = 3$  sensors communicating with sensor node  $s$ , ‘1222’ may be the next candidate which may translate into “sensor  $s$  remains stationary, and all the other three sensors translate to the right by 10 m”. The evolution of this multi-sensor command takes place based on a genetic algorithm. Each iteration of the algorithm includes three steps:

- **Reproduction:** Assuming that a population of samples (or candidate solutions), denoted by  $\mathbb{U}$  (each sample being a string and meaning one hypothesized multi-sensor command) are input from the previous iteration, for each sample  $u_s \in \mathbb{U}$ , the reward function  $v(u_s) = v(\pi_{k|k-1,s}(\cdot), \tilde{\pi}_{\text{fused},k,s}(\cdot; u_s))$  is computed. Having all the reward values, reproduction probabilities are then computed for each candidate,

$$p(u_s) = v(u_s) / \sum_{u'_s \in \mathbb{U}} v(u'_s). \quad (13)$$

The population is then resampled according to the above probabilities. The result will be a new population of the *surviving* candidate solutions who are ready for reproducing. Reproduction is conducted using a selection scheme based on the weighted roulette wheel method.

- **Crossover:** The surviving candidate solutions are paired together, and for each pair of “parent” candidate solutions, a new pair is formed via a crossover technique. We use a simple crossover method where an index from one to the length of the sample,  $1 + |N(s)|$ , is randomly chosen. Then all the coded commands at that index and after are swapped between the two multi-sensor commands (samples).
- **Mutation:** With a (usually very small) probability, each code (single-sensor command) at each sample changes to a randomly selected code among possible commands in  $\mathbb{U}$ .

As for the stopping criterion, the iterations are repeated for a fixed number of times or until the maximum reward associated with the *best* solution in the population is detected to be not improving for a specified number of successive iterations.

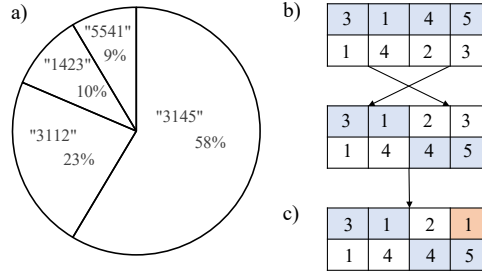


Figure 7: Three steps of the genetic algorithm: a) roulette-wheel reproduction, b) crossover, c) mutation.

A single-iteration and simplified example of the algorithm is shown in Figure 7 where the population comprises only 4 samples, each representing control command candidates for controlling the sensor node  $s$  and its three neighboring nodes. In the reproduction step, if for instance 100 samples are generated, 58 of them will be “3145”, 23 of them will be “3112”, 10 will be “1423” and 9 will be “5541”. In the crossover step, the figure shows what may happen to the pair (“3145”, “1423”), assuming that index 2 is randomly chosen so all codes indexed 2 and after are swapped between the two samples, generating a new pair. In the mutation step, it happens that one of the two samples in the pair is mutated, i.e. one code within it is randomly changed from ‘3’ to ‘1’. Note that we ended up with a final pair that is entirely different from the original pair selected from the reproducing samples, but with improved fitness values.

### Distributed Flooding-Based Multi-Sensor Control (DF-SC)

While the Genetic Algorithm method can significantly decrease the computational cost compared to the distributed coordinate descent method, particularly in a densely connected sensor network, it still only considers a sensor’s neighborhood when calculating the multi-sensor control command rather than the entire sensor network. There are non-trivial barriers to implementing a distributed control scheme where each sensor node accounts for every node’s actions, including ensuring distributed consensus and computational limitations.

We propose a flooding-based method that realizes a truly distributed, asynchronous, multi-sensor control algorithm. The basic idea is that each sensor node will iteratively update its own selected action, taking into account the actions that every other sensor has selected. In a distributed network, two sensors cannot know the other’s selected action in real-time. But they can *flood-in* the information related to the action most recently selected by others, and *flood-out* their own selection to others for future use in their own asynchronous time.

At each sensor node, an iterative operation occurs with each iteration comprised of flooding-in, optimization, and flooding-out steps. Let us denote the iteration counter for this process by  $t$ , in contrast to filtering iterations denoted by  $k$ . In iteration  $t$ , the sensor node  $s$  first receives all optimal decisions  $u_{s'}^*(t-1)$  from its neighboring sensors  $s' \in N(s)$ . That is the realization of the flood-in step. Note that communication of only the selected control commands from other nodes does not normally incur a heavy load on communication. Hence, we can practically assume that after a number flooding steps, that is dependent on the network size, each sensor node will have communicated with the entire network, or in the case of an extremely large network a large subset of the entire network. Denoting the total number of nodes in the network by  $N_s$  and using integer indices for sensor labels, e.g.  $\mathbb{S} = \{1, \dots, N_s\}$ , the optimization step of iteration  $t$  involves

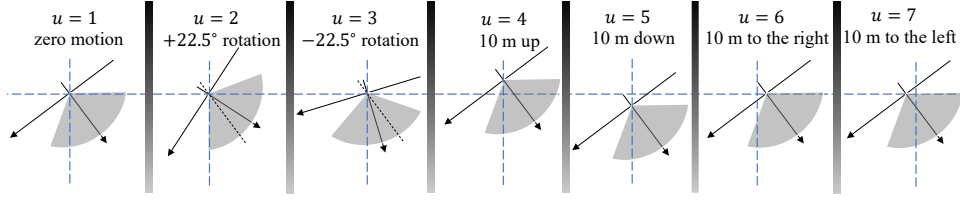


Figure 8: Possible sensor commands in the challenging case of our numerical experiments.

an exhaustive search over the space of single-sensor commands as follows:

$$u_s^*(t) = \underset{u \in \mathcal{U}}{\operatorname{argmax}} \nu(u_{1:(s-1)}^*(t-1), u, u_{(s+1):N_s}^*(t-1)) \quad (14)$$

where  $u_{1:(s-1)}^*(t-1)$  denotes the  $(s-1)$ -tuple of recent decisions made by sensor nodes  $1 : (s-1)$ , and similar definition applies to  $u_{(s+1):N_s}^*(t-1)$  i.e.

$$\begin{aligned} u_{1:(s-1)}^*(t-1) &\triangleq (u_1^*(t-1), u_2^*(t-1), \dots, u_{s-1}^*(t-1)) \\ u_{(s+1):N_s}^*(t-1) &\triangleq (u_{s+1}^*(t-1), u_{s+2}^*(t-1), \dots, u_{N_s}^*(t-1)). \end{aligned}$$

In the final step of iteration  $t$  at node  $s$ , the locally decided optimal command for the sensor is flooded-out to all the other sensor nodes for use in their own optimization step.

An important note to make here is that solving the optimization problem in equation (14) by exhaustive search is not computationally prohibitive. The main reason is that it involves computing the reward for just the finite number of possible single-sensor commands. In our numerical experiments, each sensor can execute one of the seven possible translation and rotation movements depicted in Figure 8. In addition, note that when computing the reward for each possible sensor command, PIMS calculation and pseudo update are only needed to be performed for the actual node  $s$  and not for the others.

**Stopping criterion:** Let  $u_s^*(t)$  denotes the multi-sensor command decision made at node  $s$  in iteration  $t$ . As it was explained above, we have:

$$u_s^*(t) = [u_1^*(t-1) \quad u_2^*(t-1) \quad \dots \quad u_{s-1}^*(t-1) \quad u_s^*(t) \quad u_{s+1}^*(t-1) \quad \dots \quad u_{N_s}^*(t-1)]. \quad (15)$$

The iterative process can be stopped when there is no change observed in the multi-sensor command for three consecutive iterations, i.e. when we have:

$$u_s^*(t) = u_s^*(t-1) = u_s^*(t-2). \quad (16)$$

The following lemma proves that when criterion (16) is met, all the other nodes in the network should have reached the same decision for their own and other sensors' optimal commands to be executed.

**Lemma 4.1.** *If  $\exists s \in \mathbb{S}$ ,  $u_s^*(t) = u_s^*(t-1) = u_s^*(t-2)$ , then  $\forall s' \in \mathbb{S}$ ,  $u_{s'}^*(t) = u_{s'}^*(t)$ .*

**Proof by contradiction.**

If  $\exists s' \in \mathbb{S}$ ,  $u_{s'}^*(t) \neq u_{s'}^*(t)$  then

$$\exists j \in \mathbb{S}, [j\text{-th element of } u_{s'}^*(t)] \neq [j\text{-th element of } u_s^*(t)]. \quad (17)$$

For  $j$ , there are three distinct possibilities:

- $j \neq s$  and  $j \neq s'$ : In this case, both sides of equation (17) turn out to equal  $u_j^*(t-1)$  which is contradictory.
- $j = s$ : In this case, the left and hand sides of (17) turn out to equal  $u_s^*(t-1)$  and  $u_s^*(t)$ , respectively. However, since according to (16), the multi-sensor commands  $u_s^*(t-1)$  and  $u_s^*(t)$  are equal, their  $s$ -th elements must equal too. Hence, in this case, we also hit contradiction.
- $j = s'$ : In this case, from (17) we have  $u_{s'}^*(t) \neq u_{s'}^*(t-1)$ . However, this is also contradicting equation (16) due to the reason explained below. Note that:

$$\begin{aligned} u_{s'}^*(t) &= \operatorname{argmax}_{\mathbf{u} \in \mathbb{U}} \nu\left(u_{1:(s'-1)}^*(t-1), \mathbf{u}, u_{(s'+1):N_s}^*(t-1)\right) \\ u_{s'}^*(t-1) &= \operatorname{argmax}_{\mathbf{u} \in \mathbb{U}} \nu\left(u_{1:(s'-1)}^*(t-2), \mathbf{u}, u_{(s'+1):N_s}^*(t-2)\right). \end{aligned} \quad (18)$$

On the other hand, since  $u_s^*(t) = u_s^*(t-1)$ , we have  $\forall m \in [\mathbb{S} - \{s\}], u_m^*(t-1) = u_m^*(t-2)$ , and since  $u_s^*(t-1) = u_s^*(t-2)$ , the  $s$ -th elements of the two sides are equal and therefore, for  $m = s$ , we also have  $u_m^*(t-1) = u_m^*(t-2)$ . Hence, for any  $\mathbf{u} \in \mathbb{U}$ , the input arguments of the two reward functions in (18) are equal, and consequently the search outcomes,  $u_{s'}^*(t)$  and  $u_{s'}^*(t-1)$  must equal as well, which is contradictory to the initial assumption.  $\square$

In practice, once the convergence required by the stopping criterion (16) is met at some node  $s$ , in the next iteration of information flooding, that sensor will send a signal to the other sensors, telling them that convergence is reached and they can stop and execute their optimal command. While the stopping criterion will be reached most of the time, our experiments have shown that rarely a loop may be formed where the multi-sensor control command at each node cycles through two or more states. This can be simply addressed by adding a maximum number of iterations,  $t_{\max}$ , after which the most recent control command is executed. The maximum threshold will be particularly useful in practical scenarios where due to dropout or disconnection, not every sensor node in the network can communicate with every other node.

Another practical consideration is related to the asynchronous nature of this algorithm. In practice, sensors in the center of the network require fewer flooding iterations to receive information from all communicable sensors. Thus, in each single iteration, while different nodes should take similar amounts of time to reach their newly selected control command, small variations are possible, causing some sensors to progress to the next iteration earlier. Therefore, each sensor  $s$  will have an individual iteration  $t_s$ . However, as the values of multi-sensor commands at each sensor come from other sensors at their own iterations via flooding, the fastest sensor cannot progress more than one iteration beyond the slowest sensor. In other words, at any time,

$$t_{\text{fastest node}} < t_{\text{slowest node}} + 1 \text{ filtering iteration.} \quad (19)$$

## 5. Numerical Experiments

In this section, we first describe the scenarios designed for evaluating the control methods, followed by a detailed discussion of the tested methods. The results of these scenarios are presented and analyzed.



### 5.1. Scenarios

Various scenarios were designed and simulated to assess the tracking performance of the proposed methods. The first scenario consists of 25 sensors distributed within a  $2000\text{ m} \times 2000\text{ m}$  area, tracking eight targets moving within a  $1600\text{ m} \times 1600\text{ m}$  area. These concentric areas are referred to as the sensor area and the target area. Target births occur randomly along the edges of the target area, with a trajectory directing the target inwards from the edge of the target area. Each target additionally has a 0.005 probability of death at each time step after 50. These targets follow a constant turn motion model, where the turn rate is uniformly distributed in  $\pm 0.25^\circ/\text{sec}$ .

Each sensor's detection profile is modeled by equation (2), in the form depicted in Figure 3, with  $\theta_{\max} = 45^\circ$  ( $90^\circ$  field-of-view) and maximum detection range of  $\rho_{\max} = 600\text{ m}$ . The communication range between sensors is also simulated to be at maximum 600 m.

The second scenario involves ten sensors tracking eight targets. Sensor's detection profiles are similar to the first scenario except for the maximum detection range and communication range being 1000 m and 800 m, respectively.

In both scenarios, the  $p_{\max}^d$  and  $\lambda$  parameters in equation (2), which represent the maximum probability of detection and the shape parameter, are respectively set at 0.995 and 65 m as shown in Figure 4. As shown in Figure 6, measurements are returned as a two-element vector, representing the distance from the sensor to the measurement along the x-axis and y-axis. However, unlike in Figure 6 where noise-free PIMS are shown, the simulated measurements used in the update step of the LMB filters are noisy. The variance of the white measurement noise along each axis increases with the sensor-object distance,  $\rho$ , at a rate of  $1 + (\rho/1000\text{ m})^2$ .

In all experiments, each sensor can move according to one of the seven control commands shown in Figure 8. In both scenarios, we ran 50 Monte Carlo experiments and the initial positions and orientations of sensors randomly varied from one experiment to the other. However, those random variations were constrained to ensure distributed communication would span the entire set of sensors. Figure 9 shows a sample of random initialization in one of the Monte Carlo experiments with the first scenario.

### 5.2. Methods

Three distinct RFS-based, distributed, multi-sensor control methods were evaluated: Distributed Coordinate Descent (DCD-SC) [27], the Genetic Algorithm (GA-SC) approach, and the Distributed Flooding method (DF-SC). For every method and scenario, 50 Monte Carlo experiments were conducted. In each experiment, the initial positions of sensors were sampled from a uniform distribution within the sensor area, ensuring that each sensor remained within communication range of at least one other sensor. The initial orientations of sensors were uniformly sampled from 0 to  $2\pi$ . Furthermore, sensors with fixed positions and orientations were also examined to establish baseline results.

### 5.3. Results

In these experiments, the OSPA distance error metric [50] and OSPA(2) error metric [51] were used to evaluate the multi-target tracking performance in both scenarios. Table 1 presents the results for different distributed sensor control methods, in each of the two scenarios. Comparison is made between the baseline fixed-sensor configuration (no sensor control), distributed coordinate-descent sensor control (DCD-SC), and the two proposed methods, GA-SC and DF-SC. Additionally, the average computation times for a single sensor in a single filtering time step are listed Table 2.

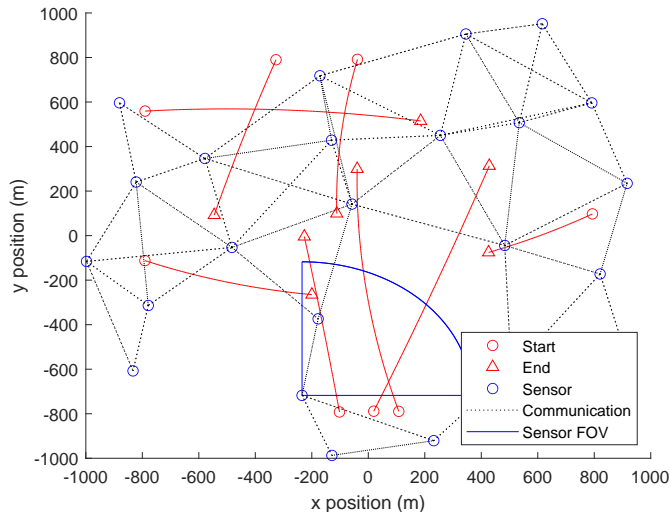


Figure 9: Overview of the 25 sensor scenario: Initial sensor positions are represented by blue circles, the FoV of one sensor is shown as an example, the presence of communication between a pair of sensors is indicated by a dotted line, and the target trajectories are denoted in red.

Table 1: Comparison of tracking performance results obtained from various multi-sensor control methods.

Scenario	Multi-sensor control method	OSPA distance	OSPA(2) distance
25 Sensors	Fixed Sensors	38.2677	49.6701
	DCD-SC	37.8815	51.4802
	GA-SC	25.3908	30.1627
	DF-SC	20.9146	31.5160
10 Sensors	Fixed Sensors	18.5507	36.9099
	DCD-SC	10.2978	34.1288
	GA-SC	14.2669	30.6080
	DF-SC	10.8594	30.1478

#### 5.4. Discussion

In the 10-sensor scenario the DCD-SC method exhibited significantly improved performance compared to the fixed sensors, however in the 25-sensor scenario it only slightly improved upon the fixed sensors. This outcome in the more challenging 25-sensor scenario can be attributed to the limited number of iterations computed for this method, which was necessary to maintain manageable computation times (yet, the average computation times reported for DCD-SC in Table 2 are much larger than other methods). In both scenarios, the GA-SC method demonstrated improved accuracy relative to the fixed sensors, although not as strongly as the DCD-SC method in the 10-sensor scenario. The DF-SC method emerged as the most accurate in the 25-sensor scenario and close to the DCD-SC method in the 10-sensor scenario, while also displaying the lowest computation time in the 25-sensor scenario and computation time comparable with the GA-SC method in the 10-sensor scenario.

The following is a comparison of the computational costs associated with each tested method. The computational complexity of the DCD-SC method [27] is  $O(m \times n \times N(s) \times |\mathcal{U}|)$ , where  $m$

Table 2: Average single-node computation times associated with different multi-sensor control methods used for distributed multi-target tracking in each of the two scenarios.

Multi-sensor control method	Scenario 1 (25 Sensors)	Scenario 2 (10 Sensors)
Fixed Sensors	0.144 s	0.120 s
DCD-SC	122.276 s	46.778 s
GA-SC	67.529 s	10.789 s
DF-SC	30.251 s	10.935 s

represents the number of runs,  $n$  is the number of iterations per run,  $N(s)$  is the number of sensors in the neighborhood of sensor  $s$ , and  $|\mathbb{U}|$  is the number of possible control commands. The computational complexity of the GA-SC method is given by  $\mathcal{O}(m \times n_s)$ , where  $m$  denotes the number of iterations and  $n_s$  is the size of the population at sensor  $s$ . The computational complexity of the DF-SC method is expressed as  $\mathcal{O}(m \times |\mathbb{U}|)$ , with  $m$  being the number of iterations and  $|\mathbb{U}|$  representing the number of possible control commands.

On average, for the same number of runs until convergence, DCD-SC is computationally  $n N(s)$  times heavier than DF-SC. Such a comparison between DF-SC and GA-SC is more complex since determining the number of iterations and population size required for a specific level of performance using GA-SC is difficult based on known variables such as  $n_s$  and  $|\mathbb{U}|$ . Nevertheless, in terms of computational power, DF-SC is generally favored over GA-SC when there are fewer sensors in the entire network. Conversely, GA-SC is more favored when the sensor network is less densely connected and when there are fewer potential sensor actions.

## 6. Conclusion

This paper addresses the problem of multi-sensor control in a distributed sensor network with a focus on multi-target tracking applications. Two control methods, namely Genetic Algorithm (GA-SC) and Distributed Flooding (DF-SC), were proposed and subsequently compared to the Distributed Coordinate Descent (DCD) method. To evaluate the tracking performance of these methods, two scenarios with varying sensor and target numbers were designed, and the OSPA distance and OSPA(2) error metrics were employed.

The results demonstrated that the DF-SC method matched or outperformed the other methods in terms of accuracy and computational time for both scenarios. The performance of the DCD-SC method was found to be similar to that of fixed sensors in the 25-sensor scenario, which could be attributed to the limited number of iterations computed for this method. The GA-SC method exhibited improved accuracy over fixed sensors in both scenarios. Notably, the DF-SC method emerged almost as accurate as the DCD-SC method in the 10-sensor scenario, while exhibiting comparable computation time as the GA-SC method, and emerged as the most accurate in the 25-sensor scenario while also exhibiting the lowest computation time.

Upon comparing the computational complexity of the tested methods, it was determined that DF-SC is computationally advantageous over DCD-SC and GA-SC under specific conditions, primarily when there are fewer sensors in the network and when the sensor network is less densely connected. Further research into the effect that these network parameters as well as the construction of the Genetic Algorithm (such as the crossover function) have on performance may be useful. As a direction for future research, adaptive methods that dynamically adjust the control parameters based on tracking performance and network density could be explored.

## Acknowledgment

The Australian Research Council supported this work through Grant DE210101181.

## References

- [1] H. H. T. Liu, B. Zhu, Formation Control of Multiple Autonomous Vehicle Systems, John Wiley & Sons, Ltd, 2018. URL: <https://onlinelibrary.wiley.com/doi/abs/10.1002/9781119263081.ch4>. doi:<https://doi.org/10.1002/9781119263081.ch4>. arXiv:<https://onlinelibrary.wiley.com/doi/pdf/10.1002/9781119263081.ch4>.
- [2] G. Mitchell, J. Mazurek, K. Theriault, P. Manghwani, Distributed Sensor Networks, Chapman and Hall/CRC, 2013.
- [3] F. Lian, L. Hou, J. Liu, C. Han, Constrained multi-sensor control using a multi-target mse bound and a  $\delta$ -glmb filter, Sensors 18 (2018). URL: <https://www.mdpi.com/1424-8220/18/7/2308>. doi:10.3390/s18072308.
- [4] N. Truong, U. Jayasinghe, T.-W. Um, G. M. Lee, A survey on trust computation in the internet of things, THE JOURNAL OF KOREAN INSTITUTE OF COMMUNICATIONS AND INFORMATION SCIENCES (J-KICS) 33 (2016) 10–27.
- [5] G. Coulouris, J. Dollimore, T. Kindberg, Distributed Systems: Concepts and Design, International computer science series, Addison-Wesley, 2005.
- [6] L. Xiao, S. Boyd, S. Lall, A scheme for robust distributed sensor fusion based on average consensus, in: IPSN 2005. Fourth International Symposium on Information Processing in Sensor Networks, 2005., IEEE, 2005, pp. 63–70.
- [7] G. Battistelli, L. Chisci, C. Fantacci, A. Farina, R. P. S. Mahler, Distributed fusion of multitarget densities and consensus PHD/CPHD filters, in: I. Kadar (Ed.), Signal Processing, Sensor/Information Fusion, and Target Recognition XXIV, volume 9474, International Society for Optics and Photonics, SPIE, 2015, p. 94740E. URL: <https://doi.org/10.1117/12.2176948>. doi:10.1117/12.2176948.
- [8] T. Li, J. M. Corchado, J. Prieto, Convergence of distributed flooding and its application for distributed bayesian filtering, IEEE Transactions on Signal and Information Processing over Networks 3 (2017) 580–591. doi:10.1109/TSIPN.2016.2631944.
- [9] T. Li, X. Wang, Y. Liang, Q. Pan, On arithmetic average fusion and its application for distributed multi-bernoulli multitarget tracking, IEEE Transactions on Signal Processing 68 (2020) 2883–2896. doi:10.1109/TSP.2020.2985643.
- [10] R. Mahler, Statistical Multisource-Multitarget Information Fusion, 2007.
- [11] B.-T. Vo, B.-N. Vo, A. Cantoni, The cardinality balanced multi-target multi-bernoulli filter and its implementations, IEEE Transactions on Signal Processing 57 (2008) 409–423.
- [12] B. T. Vo, B. N. Vo, Labeled random finite sets and multi-object conjugate priors, IEEE Transactions on Signal Processing 61 (2013) 3460–3475. doi:10.1109/TSP.2013.2259822. arXiv:arXiv:1312.2372v1.
- [13] B. N. Vo, B. T. Vo, D. Phung, Labeled random finite sets and the Bayes multi-target tracking filter, IEEE Transactions on Signal Processing 62 (2014) 6554–6567. doi:10.1109/TSP.2014.2364014.
- [14] S. Reuter, A. Scheel, K. Dietmayer, The multiple model labeled multi-bernoulli filter, in: 2015 18th International Conference on Information Fusion (Fusion), IEEE, 2015, pp. 1574–1580.
- [15] B. Wei, L. Zhou, Cell lineage tracking based on labeled random finite set filtering, in: 2018 International Conference on Control, Automation and Information Sciences (ICCAIS), 2018, pp. 163–168. doi:10.1109/ICCAIS.2018.8570327.
- [16] N. Ishtiaq, A. K. Gostar, A. Bab-Hadiashar, R. Hoseinnezhad, Interaction-aware labeled multi-bernoulli filter, 2022. URL: <https://arxiv.org/abs/2204.08655>. doi:10.48550/ARXIV.2204.08655.
- [17] R. P. S. Mahler, Advances in statistical multisource-multitarget information fusion, 2014.
- [18] L. Gao, G. Battistelli, L. Chisci, Fusion of labeled rfs densities with minimum information loss, IEEE Transactions on Signal Processing 68 (2020) 5855–5868. doi:10.1109/TSP.2020.3028496.
- [19] B. Ristic, B.-N. Vo, Sensor control for multi-object state-space estimation using random finite sets, Automatica 46 (2010) 1812–1818. URL: <https://www.sciencedirect.com/science/article/pii/S0005109810002955>. doi:<https://doi.org/10.1016/j.automatica.2010.06.045>.
- [20] A. K. Gostar, R. Hoseinnezhad, A. Bab-Hadiashar, Multi-bernoulli sensor control via minimization of expected estimation errors, IEEE Transactions on Aerospace and Electronic Systems 51 (2015) 1762–1773. doi:10.1109/TAES.2015.140211.
- [21] M. Beard, B.-T. Vo, B.-N. Vo, S. Arulampalam, Sensor control for multi-target tracking using cauchy-schwarz divergence, in: 2015 18th International Conference on Information Fusion (Fusion), 2015, pp. 937–944.

- [22] H. G. Hoang, B. T. Vo, Sensor management for multi-target tracking via multi-bernoulli filtering, *Automatica* 50 (2014) 1135–1142. URL: <https://www.sciencedirect.com/science/article/pii/S0005109814000454>. doi:<https://doi.org/10.1016/j.automatica.2014.02.007>.
- [23] M. Jiang, W. Yi, L. Kong, Multi-sensor control for multi-target tracking using cauchy-schwarz divergence, in: 2016 19th International Conference on Information Fusion (FUSION), 2016, pp. 2059–2066.
- [24] X. Wang, R. Hoseinnezhad, A. K. Gostar, T. Rathnayake, B. Xu, A. Bab-Hadiashar, Multi-sensor control for multi-object bayes filters, *Signal Processing* 142 (2018) 260–270. URL: <https://www.sciencedirect.com/science/article/pii/S0165168417302773>. doi:<https://doi.org/10.1016/j.sigpro.2017.07.031>.
- [25] S. Panicker, A. K. Gostar, A. Bab-Hadiashar, R. Hoseinnezhad, Tracking of targets of interest using labeled multi-bernoulli filter with multi-sensor control, *Signal Processing* 171 (2020) 107451. URL: <https://www.sciencedirect.com/science/article/pii/S016516841930502X>. doi:<https://doi.org/10.1016/j.sigpro.2019.107451>.
- [26] N. Ishtiaq, S. Panicker, A. K. Gostar, A. Bab-Hadiashar, R. Hoseinnezhad, Selective Sensor Control via Cauchy Schwarz Divergence, Springer, 2021, pp. 113–124. doi:10.1007/978-981-15-5224-3\_11.
- [27] A. Blair, A. K. Gostar, R. Tennakoon, A. Bab-Hadiashar, X. Li, J. Palmer, R. Hoseinnezhad, Distributed multi-sensor control for multi-target tracking, in: International Conference on Control, Automation and Information Sciences (ICCAIS 2022), 2022, p. 72. doi:10.1117/12.2637606.
- [28] T. Rathnayake, A. Khodadadian Gostar, R. Hoseinnezhad, R. Tennakoon, A. Bab-Hadiashar, On-line visual tracking with occlusion handling, *Sensors* 20 (2020). URL: <https://www.mdpi.com/1424-8220/20/3/929>, ISSN={1424-8220}, DOI={10.3390/s20030929}.
- [29] S. Panicker, A. K. Gostar, A. Bab-Hadiashar, R. Hoseinnezhad, Sensor control for selective object tracking using labeled multi-bernoulli filter, in: 2018 21st International Conference on Information Fusion (FUSION), 2018, pp. 2218–2224. doi:10.23919/ICIF.2018.8455829.
- [30] A. K. Gostar, T. Rathnayake, R. Tennakoon, A. Bab-Hadiashar, G. Battistelli, L. Chisci, R. Hoseinnezhad, Centralized cooperative sensor fusion for dynamic sensor network with limited field-of-view via labeled multi-bernoulli filter, *IEEE Transactions on Signal Processing* 69 (2021) 878–891. doi:10.1109/TSP.2020.3048595.
- [31] A. K. Gostar, T. Rathnayake, R. Tennakoon, A. Bab-Hadiashar, G. Battistelli, L. Chisci, R. Hoseinnezhad, Cooperative sensor fusion in centralized sensor networks using cauchy-schwarz divergence, *Signal Processing* 167 (2020) 107278. URL: <https://www.sciencedirect.com/science/article/pii/S0165168419303329>. doi:<https://doi.org/10.1016/j.sigpro.2019.107278>.
- [32] C. Fantacci, B. N. Vo, B. T. Vo, G. Battistelli, L. Chisci, Consensus labeled random finite set filtering for distributed multi-object tracking, 2015. URL: <https://arxiv.org/abs/1501.01579>. doi:10.48550/ARXIV.1501.01579.
- [33] J. Klupacs, A. K. Gostar, T. Rathnayake, I. Gondal, A. Bab-Hadiashar, R. Hoseinnezhad, Multi-sensor fusion for connected driving: A review, Unpublished (2022).
- [34] D. Akselrod, T. Kirubarajan, Collaborative distributed sensor management and information exchange flow control for multitarget tracking using Markov decision processes, in: I. Kadar (Ed.), *Signal Processing, Sensor Fusion, and Target Recognition XVII*, volume 6968, International Society for Optics and Photonics, SPIE, 2008, pp. 165–175. URL: <https://doi.org/10.1117/12.779348>. doi:10.1117/12.779348.
- [35] Y. Fu, L. Yang, Sensor mobility control for multitarget tracking in mobile sensor networks, *International Journal of Distributed Sensor Networks* 10 (2014) 278179. URL: <https://doi.org/10.1155/2014/278179>. doi:10.1155/2014/278179. arXiv:<https://doi.org/10.1155/2014/278179>.
- [36] Q. Yuan, J. Zhan, X. Li, Outdoor flocking of quadcopter drones with decentralized model predictive control, *ISA Transactions* 71 (2017) 84–92. URL: <https://www.sciencedirect.com/science/article/pii/S0019057817304895>. doi:<https://doi.org/10.1016/j.isatra.2017.07.005>, special issue on Distributed Coordination Control for Multi-Agent Systems in Engineering Applications.
- [37] W. Zhou, Z. Liu, J. Li, X. Xu, L. Shen, Multi-target tracking for unmanned aerial vehicle swarms using deep reinforcement learning, *Neurocomputing* 466 (2021) 285–297. URL: <https://www.sciencedirect.com/science/article/pii/S0925231221014223>. doi:<https://doi.org/10.1016/j.neucom.2021.09.044>.
- [38] S. J. Wright, Coordinate descent algorithms, 2015. URL: <https://arxiv.org/abs/1502.04759>. doi:10.48550/ARXIV.1502.04759.
- [39] P. Richtárik, M. Takáč, Distributed coordinate descent method for learning with big data, 2013. URL: <https://arxiv.org/abs/1310.2059>. doi:10.48550/ARXIV.1310.2059.
- [40] Z. Yang, W. U. Bajwa, Byrdie: Byzantine-resilient distributed coordinate descent for decentralized learning, *CoRR* abs/1708.08155 (2017). URL: <http://arxiv.org/abs/1708.08155>. arXiv:1708.08155.
- [41] D. E. Goldberg, *Genetic Algorithms in Search, Optimization, and Machine Learning*, Addison-Wesley, New York, 1989.
- [42] L. Hua, J. Zhang, D. Li, X. Xi, M. Shah, Sensor fault diagnosis and fault tolerant control of quadrotor uav based on genetic algorithm, *Journal of Sensors* 2022 (2022) 1–8. doi:10.1155/2022/8626722.

- [43] J. Ruan, C. Zhang, Y. Li, P. Li, Z. Yang, X. Chen, M. Huang, T. Zhang, Improving the efficiency of dissolved oxygen control using an on-line control system based on a genetic algorithm evolving fwnn software sensor, *Journal of Environmental Management* 187 (2017) 550–559. URL: <https://www.sciencedirect.com/science/article/pii/S0301479716308581>. doi:<https://doi.org/10.1016/j.jenvman.2016.10.056>.
- [44] J. Jia, J. Chen, G. Chang, Z. Tan, Energy efficient coverage control in wireless sensor networks based on multi-objective genetic algorithm, *Computers & Mathematics with Applications* 57 (2009) 1756–1766. URL: <https://www.sciencedirect.com/science/article/pii/S089812210800552X>. doi:<https://doi.org/10.1016/j.camwa.2008.10.036>, proceedings of the International Conference.
- [45] R. P. Mahler, T. R. Zajic, Probabilistic objective functions for sensor management, in: *Signal Processing, Sensor Fusion, and Target Recognition XIII*, volume 5429, SPIE, 2004, pp. 233–244.
- [46] A. K. Gostar, R. Hoseinnezhad, A. Bab-Hadiashar, Multi-Bernoulli sensor-selection for multi-target tracking with unknown clutter and detection profiles, *Signal Processing* 119 (2016) 28–42. URL: <https://www.sciencedirect.com/science/article/pii/S0165168415002339>. doi:<https://doi.org/10.1016/j.sigpro.2015.07.007>.
- [47] A. K. Gostar, R. Hoseinnezhad, A. Bab-Hadiashar, Robust multi-bernoulli sensor selection for multi-target tracking in sensor networks, *IEEE Signal Processing Letters* 20 (2013) 1167–1170. doi:10.1109/LSP.2013.2283735.
- [48] T. van Erven, P. Harremoës, Rényi divergence and kullback-leibler divergence, *IEEE Transactions on Information Theory* 60 (2014) 3797–3820.
- [49] K. Shen, C. Zhang, P. Dong, Z. Jing, H. Leung, Consensus-based labeled multi-Bernoulli filter with event-triggered communication, *IEEE Transactions on Signal Processing* 70 (2022) 1185–1196. doi:10.1109/TSP.2022.3154227.
- [50] D. Schuhmacher, B.-T. Vo, B.-N. Vo, A consistent metric for performance evaluation of multi-object filters, *IEEE Transactions on Signal Processing* 56 (2008) 3447–3457. doi:10.1109/TSP.2008.920469.
- [51] M. Beard, B. T. Vo, B.-N. Vo, Ospa(2): Using the ospa metric to evaluate multi-target tracking performance, in: *2017 International Conference on Control, Automation and Information Sciences (ICCAIS)*, 2017, pp. 86–91. doi:10.1109/ICCAIS.2017.8217598.